Hydrogen Storage with Aluminum Formate, ALF: Experimental, Computational and Technoeconomic Studies

Hayden A. Evans[1]*, Taner Yildirim[1]*, Peng Peng[2], Yongqiang Cheng[3], Zeyu Deng[4], Qiang Zhang[3], Dinesh Mullangi[4], Dan Zhao[5], Piero Canepa[4], Hanna Bruenig[2], Anthony K. Cheetham[4,6], Craig. M. Brown[1]*

1. Center for Neutron Research, National Institute of Standards and Technology, Gaithersburg, Maryland, USA
2. Energy Analysis and Environmental Impacts Division, Lawrence Berkeley National Laboratory, Berkeley, CA, USA
3. Neutron Scattering Division, Oak Ridge National Laboratory, Oak Ridge, Tennessee, USA
4. Department of Materials Science and Engineering, National University of Singapore, 9 Engineering Drive 1, Singapore
5. Department of Chemical and Biomolecular Engineering, National University of Singapore, Singapore
6. Materials Research Laboratory, University of California; Santa Barbara, California, USA

*Corresponding Authors : hayden.evans@nist.gov, taner.yildirim@nist.gov, craig.brown@nist.gov

Keywords: Hydrogen storage, ReO_3-type material, Neutron diffraction, Technoeconomic analysis

Abstract

Long-duration storage of hydrogen is necessary for coupling renewable H_2 with stationary fuel cell power applications. In this work, aluminum formate (ALF), which adopts the ReO_3-type structure, is shown to have remarkable H_2 storage performance at non-cryogenic (>120 K) temperatures and low pressures. The most promising performance of ALF is found between 120 K and 160 K and 10 bar to 20 bar. The study illustrates H_2 adsorption performance of ALF over the 77 K to 296 K temperature range using gas isotherms, in-situ neutron powder diffraction, DFT calculations, as well as technoeconomic analysis (TEA) illustrating ALF's competitive performance for long-duration storage versus compressed hydrogen and leading metal-organic frameworks (MOFs). In the TEA, it is shown that ALF's storage capacity, when combined with a temperature/pressure swing process, has advantages versus compressed H_2 at a fraction of the pressure (15 bar versus 350 bar). Given ALF's performance in the 10 bar to 20 bar regime under moderate cooling, it is particularly promising for use in safe storage systems serving fuel cells.

Introduction

Stationary hydrogen-powered fuel cells are an emerging solution for delivering clean and flexible power.[1–3] Renewable energy powered electrolysis can generate hydrogen, but may require multiple days' worth of hydrogen storage to smooth renewable energy variability. Storage is also needed in cases where hydrogen is used as a backup power system, with a necessary target storage duration of 96 hours to meet the requirements set by the United States National Fire Protection Association. This presents a challenge, as compressed gas or cryogenic hydrogen storage is operationally expensive and inefficient at large scales for these storage durations, and salt caverns proposed for storage are not widely available and require pipelines to make them suitable for significantly larger applications. As such, much work has been conducted to identify material-based solutions for hydrogen storage that operate at lower pressures and warmer temperatures.

A recent analysis by some of the authors of stationary hydrogen storage for long-duration energy supply suggests there is potential for porous metal-organic frameworks (MOFs) to perform well in such applications.[4] These materials can adsorb H_2 within their porous structures, and via gas-framework interactions, facilitating high hydrogen storage capacities. However, a MOF's peak adsorption under equilibrium conditions is only one indicator of promise, and a

https://doi.org/10.26434/chemrxiv-2023-7b1m5 **ORCID:** https://orcid.org/0000-0002-1331-4274 Content not peer-reviewed by ChemRxiv. **License:** CC BY-NC-ND 4.0

MOF must be holistically evaluated across other key factors, such as the constraints resulting from integration with electrolyzer and fuel cell systems. Fuel cells require high-purity hydrogen at fast delivery rates and modest pressures, which MOFs are uniquely capable of achieving. Additionally, previous studies have shown that green H_2 generated by on-site electrolysers tends to be warm (≈ 320 K or above),[5] and if this H_2 needed to be quenched to cryogenic temperatures (i.e., 77 K) for storage, the process would prove economically unviable.

Until recently, conventional MOFs for hydrogen storage required low temperatures to achieve high hydrogen uptake.[6,7] Most reported MOFs (e.g., $Zn_4O(BDC)_3$ (MOF-5, BDC^{2-} = 1,4-benzenedicarboxylate) and $Cu_3(BTC)_2$ (HKUST-1, BTC^{3-} = 1,3,5-benzenetricarboxylate)), show maximum hydrogen uptake under cryogenic temperature and high-pressure conditions, whereas some emerging MOFs, such as Ni_2(*m*-dobdc) and V-btdd (*m*-$dobdc^{4-}$ = 4,6-dioxido-1,3-benzenedicarboxylate; H_2btdd, bis(1*H*-1,2,3-triazolo[4,5-*b*],[4′,5′-*i*])dibenzo[1,4]dioxin), exhibit record deliverable H_2 at near-ambient temperatures and high-pressure conditions (i.e., above 100 bar).[8,9] Initial findings suggested that Ni_2(*m*-dobdc) could achieve a lower levelized cost of storage ($/kWh) relative to cryogenic storage, but not compared to compressed gas storage at 350 bar without Ni_2(*m*-dobdc) being made cheaply and able to retain relatively high hydrogen uptake (i.e., below 10 $/kg and above 15 g/kg excess uptake).[4] It was also found that slower charging of the storage tank greatly reduced the cost of associated compression and refrigeration units, further improving the promise of sorbent-based systems.

Recently, work published by researchers here has illustrated the impressive adsorptive properties of one of the simplest and lowest-cost MOF materials, aluminum formate, $Al(HCOO)_3$ (ALF). ALF adopts an ReO_3-type structure[10] and has been shown to adsorb CO_2 from dried CO_2-rich flue gas conditions with high CO_2/N_2 selectivity,[11] to selectively adsorb CO_2 from any hydrocarbon mixture, including acetylene,[12] and provides impressive selective O_2 adsorption characteristics from O_2/N_2 mixtures above cryogenic temperatures.[13] ALF also has very practical attributes sought for industrially utilized materials, such as withstanding pelletization, being air-stable, and being derived from cheap commodity chemicals.[11] Given the remarkable performance of ALF in these important areas, as well as its alluring scalability attributes, we extended our focus to examine whether ALF could be utilized for stationary hydrogen-powered fuel cell applications.

Herein, we demonstrate that ALF displays remarkable H_2 storage performance above cryogenic temperatures (> 120 K), with the most promising performance between 120 K and 160 K. We discuss the H_2 adsorption performance of ALF over the temperature ranges from 77 K to 296 K via gas isotherms, the crystal-structure of ALF as it adsorbs D_2 gas, as resolved from in-situ neutron powder diffraction, DFT calculations that support the observed performance, and technoeconomic analysis illustrating ALF's price competitive performance versus leading MOFS and compressed hydrogen for long-term storage. For the technoeconomic analysis, we show how the storage capacity of ALF, when combined with a temperature/pressure swing process, has clear advantages versus compressed H_2 at a fraction of the pressure.

Results and discussion

Gas isotherm measurements

Figure 1 displays the excess gas adsorption/desorption isotherm measurements of ALF at various temperatures plotted as a function of grams of H_2 adsorbed versus kg of ALF. The Supporting Information contains the same data plotted with other metrics, as well as the total adsorption plots, for comparison (Figures S1 – S5). As can be seen from Figure 1, ALF shows excess adsorption of H_2 gas of ≈11 grams of H_2 per kg of ALF near 120 K and ≈25 bar of pressure. As temperature is increased, the maximum adsorption decreased, as is expected from thermodynamics. Each of the isotherms can be described as Type I isotherms, and from non-linear Langmuir fits of the excess isotherms

https://doi.org/10.26434/chemrxiv-2023-7b1m5 **ORCID:** https://orcid.org/0000-0002-1331-4274 Content not peer-reviewed by ChemRxiv. **License:** CC BY-NC-ND 4.0

(Figure S6), the experimental heat of adsorption for the H_2 adsorption is 8.67 kJ/mol when treated with a single site Langmuir model. Alternative treatment using a dual-site Langmuir model with lower and

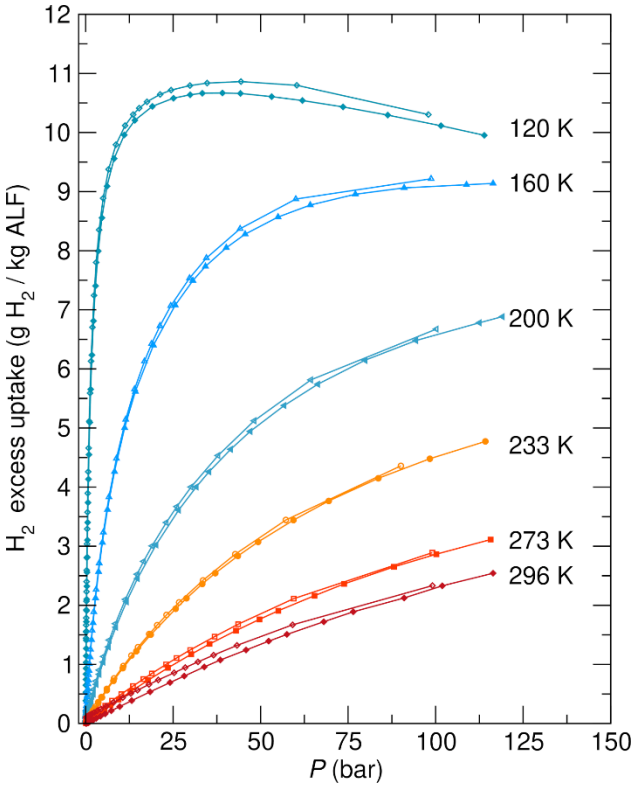

Figure 1. Excess H_2 gas adsorption/desorption isotherm measurements on ALF between 120 K and 296 K. Closed symbols = adsorption, open symbols = desorption. The same data, plotted on the y-axis with other metrics are provided in the Supporting Information, alongside total adsorption plots and non-linear Langmuir fits (Figures S1 – S5, S19 - S20).

upper bound pore volume considerations can also be found in the Supporting Information. The dual-site treatments provide similar heat of adsorption values between ≈ 8.5 kJ/mol and ≈ 9 kJ/mol as a function of loading. Given the dense, ultramicroporous nature of ALF, when compared to many large pore MOFs, the adsorption values at increased pressures trend closer to values for compressed hydrogen. Figure S7 illustrates this point by showing the observed volumetric H_2 storage densities for ALF versus theoretical compressed H_2 volumetric densities (NIST web book)[14] of a given pressure and temperature swing process ending at 5 bar and 296 K. As such, the large initial H_2 adsorption at temperatures between 120 K and 200 K and pressures beneath 50 bar offer promising performance for H_2 storage using ALF.

As temperature is decreased beneath 120 K (Figure S1 – S5), the inherent kinetic effects of ALF grow more pronounced, manifesting as hysteresis between adsorption and desorption curves. We have observed this phenomenon for both CO_2 and O_2 adsorption with ALF,[11,13] albeit at different temperatures given the distinct interactions each gas has with ALF. This kinetic behaviour, though curious, is not uncommon for microporous systems and has been observed in such systems as zeolite type A,[15] and a non-ReO_3-type Mn(II)-formate.[16] Both materials, much like ALF, display complex sorbate-framework interactions that impact adsorption kinetics. In the case of the Mn(II)-formate material, the authors postulated that the material has "*dynamic opening of the pore aperture and/or sufficient kinetic energy of the adsorbates to overcome a diffusion barrier above a critical temperature.*" We believe that there is a similar effect in ALF and that there is likely a "critical gating temperature" which is dependent on the nature of each specific gas adsorbed into ALF.

https://doi.org/10.26434/chemrxiv-2023-7b1m5 **ORCID:** https://orcid.org/0000-0002-1331-4274 Content not peer-reviewed by ChemRxiv. **License:** CC BY-NC-ND 4.0

In-situ D_2 gas dosing powder neutron diffraction studies

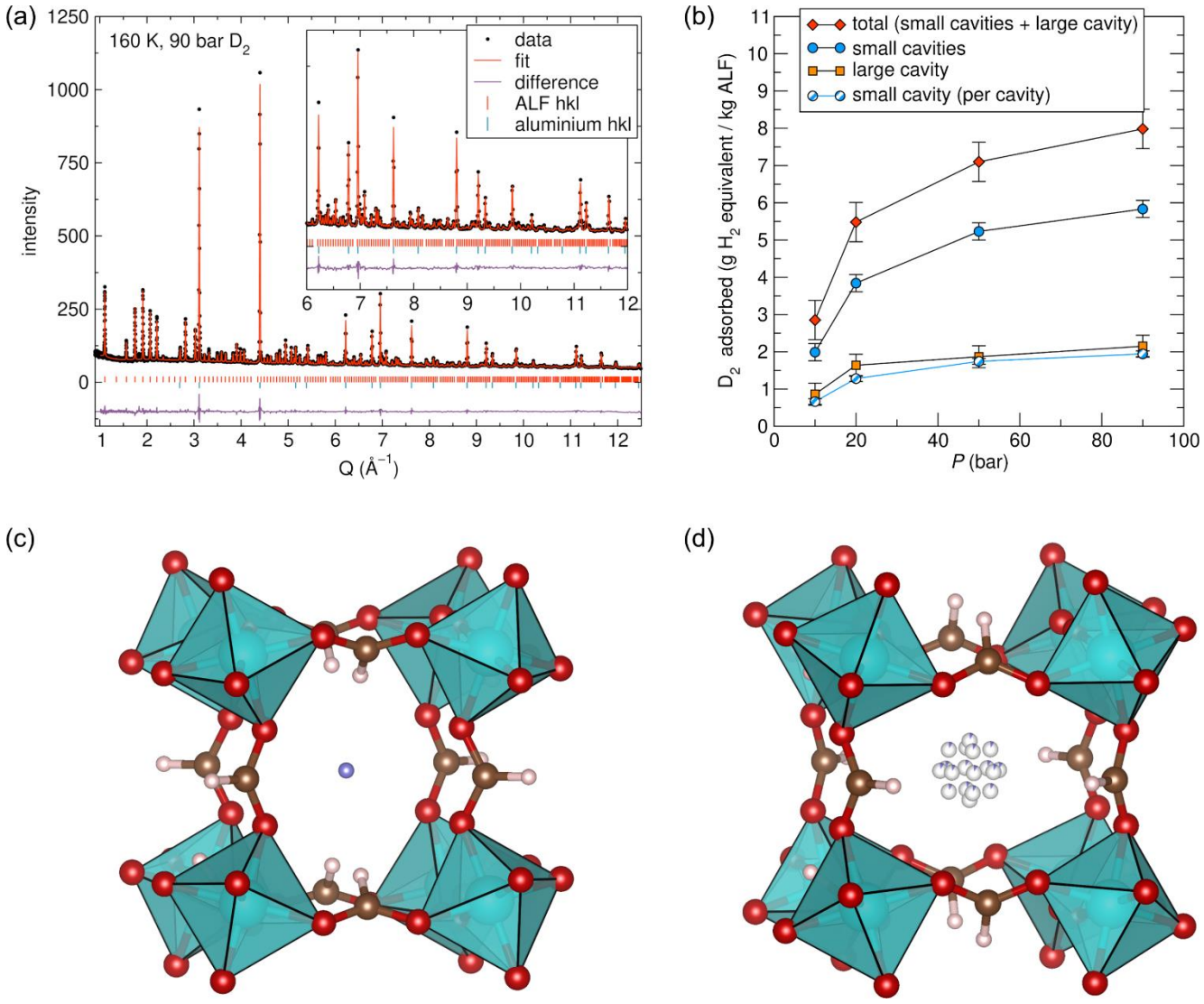

Figure 2. In-situ neutron diffraction results on ALF at 160 K under D_2 pressure. [ORNL, POWGEN]. (a) Representative Rietveld refinement of ALF under 90 bar of D_2. R_{wp} = 3.92 %, R_p = 3.37 %. Space group = 204 ($Im\bar{3}$). Lattice parameters, $a = b = c$ = 11.3669(1) Å. Aluminum hkl's refer to solid Al high-pressure sample can used for experiment, not Al metal within the sample. Other refinement results can be found in the Supporting Information, Figures S8 – S11. (b) Refined values of D_2 occupancy found within ALF from the 160 K data sets for each cavity, converted into equivalent grams of H_2 per kg of ALF (using molecular mass of 2 g/mol instead of 4 g/mol (D_2)) for direct comparison with Figure 1. These results are also shown in the Supporting Information (Figure S13) as a function of mmol D_2 / g ALF and g D_2 / kg ALF. Error bars and values denote 1 sigma. (c) Small cavity, SC, of ALF with D_2 super-atom at the centre of the cavity. (d) Large Cavity, LC, of ALF with D super-atom disordered over the surface of a sphere (radius = 0.677 Å).

In-situ D_2-dosed neutron powder diffraction experiments on ALF were conducted at the POWGEN instrument at Oak Ridge National Laboratory. Experiments were conducted at 160 K under multiple pressures of D_2 gas (0 bar, 10 bar, 20 bar, 50 bar, 90 bar) to resolve how the structure of ALF filled and/or changed with D_2 gas. The 160 K temperature was chosen for the experiments as adsorption was known to be both fast and in high enough quantities

https://doi.org/10.26434/chemrxiv-2023-7b1m5 **ORCID:** https://orcid.org/0000-0002-1331-4274 Content not peer-reviewed by ChemRxiv. **License:** CC BY-NC-ND 4.0

to ensure that reliable positions of the D_2 molecules could be located within the allotted experimental time frame. Furthermore, given the fast onset of H_2 adsorption at 120 K, conducting the experiments at 160 K also allowed incremental observation of the adsorption of D_2 into the structure of ALF to be done more precisely.

As discussed in previous work, ALF adopts an ReO_3-type structure.[10] It is akin to the perovskite structure, only instead of an *A*-site cation, there is a vacancy (void space). The structure of ALF is found in the $\boldsymbol{Im\bar{3}}$ space group, and as a result, has two crystallographically distinct cavities, denoted as the small (SC) and large cavities (LC), which differ by how the hydrogens of the formates point toward, or away, from the centre of each cavity, respectively. For CO_2 adsorption, the SC favours CO_2 adsorption relative to the LC because the hydrogen bonding from the formate hydrogens engages in a "hand-in-glove" interaction with CO_2. This contrasts what was observed for O_2 adsorption in ALF, where hydrogen bonding in the small cavity is found to be less significant, with a slight preference for the LC.[13] This slight preference for the large cavity is observed here for D_2 adsorption as well, as we will now discuss.

Figure 2 shows select results from the in-situ gas-dosed neutron powder diffraction experiments, including visualization of the D_2 positioning within the crystal structure of ALF obtained from Rietveld-derived chemical models. Figure 2(a) shows a representative Rietveld refinement fit of the data acquired for the highest dosed D_2 condition, 90 bar. This data set was used to confidently resolve the positions of the D_2 gas molecules adsorbed within ALF, which were then used for the lower pressure data sets. The Supporting Information shows the refinement fits obtained for the other pressures tested (0 bar, 10 bar, 20 bar, 50 bar). Specific to the refinements, the gas molecules were modelled as "super-atoms," given that D_2 is a quantum object and the molecular dumbbell is orientationally averaged to produce a more spherical scattering centre as is typically observed in the literature.[9,17–20] Practically, this means an appropriate Rietveld refinement will use a single D atom, instead of a D_2 molecule, to describe a D_2 molecular position. In the refinements, each D super-atom was allowed a maximum occupancy of 2 to account for the modelling of a D_2 molecule.

Figure 2(b) shows the refined amounts of D_2 adsorbed in ALF as derived from the Rietveld refinements over the range of pressures. The amounts graphed are the total amount adsorbed at each pressure, as well as the amount for each cavity. The occupancies in Figure 2(b) have been converted to grams of H_2 per kg of ALF, for direct comparison with the isotherm data in Figure 1. The metrics in mmol of D_2 per g of ALF, and g of D_2 per kg of ALF, are also found in the Supporting Information (Figure S13). The Supporting Information Tables S4 – S7 show the crystallographic occupancies from the refinements prior to conversion. As can be appreciated, the power of the in-situ gas dosing neutron diffraction experiments is that the Rietveld refinements with such data provide a real-space context as to how gases interact with an adsorbent.[21] In this instance, we found that at all D_2 pressures tested, and given that ALF has two distinct cavities, the SC and LC, both cavities adsorbed D_2 gas at near equal amounts after equilibration when normalized for multiplicity. This is shown in Figure 2(b) when comparing the D_2 occupancy of the LC versus the D_2 occupancy found in just one SC (there are three times as many SCs versus LCs within ALF, given the *Im*-3 symmetry).

Though D_2 is adsorbed into each of the cavities at near equal proportions, how the D_2 molecules fill within the two cavities is distinct. Figures 2(c) and (d) illustrate how the D super-atoms are found within the SCs and LCs, respectively, as resolved from the Rietveld refinement with the data at 160 K and 90 bar D_2 pressure. The small cavity D super-atom was found to be best modelled with one position at the special position [0, 1/2 ,0], which is the centre of the small cavity. Attempts were made to move the super-atom off this special position within the small cavity, which in principle could describe any preferential positioning within the cavity. However, no position away from the [0, 1/2, 0] position was found to statistically improve the fit or provide any other convincing indications of localization. Instead, the most stable and statistically consistent result was modelled with super atom at the centre of the cavity with a large isotropic Debye-Waller factor B_{eq} (refined and stable B_{eq} value of ≈14 $Å^2$). This result implies that the D_2 inside of the small cavity is on average localized at the centre of the cavity, albeit likely somewhat dynamic under these conditions.

This result contrasts with what was found to be the case for the large cavity, where if the D super-atoms were modelled at the centre of the large cavity, they had a similar refined B_{eq} of ≈14.2 $Å^2$ to that of the small cavity D super

https://doi.org/10.26434/chemrxiv-2023-7b1m5 **ORCID:** https://orcid.org/0000-0002-1331-4274 Content not peer-reviewed by ChemRxiv. **License:** CC BY-NC-ND 4.0

atom. However, if they were displaced from the special position so as to populate the surface of sphere inside of the large cavity, the B_{eq} values of the D super-atoms reduced and stabilized by an order of magnitude to ≈1.7 Å^2. This spherical surface modelling is shown in Figure 2(d). This indicates that there is preferential adsorption of the D_2 gas towards the surfaces of the large cavity walls/ligands, as opposed to occupying the centre of the cavity. The distinction in the localization of D_2 within the two cavities can be rationalized given that there is likely vibrational movement of the formates/formate hydrogens at these temperatures that would constantly perturb the location of the D_2 molecules when at the centre of the small cavity. Given that the large cavity has no such formate hydrogens that point inward, the D_2 molecules could be expected to be comparatively undisturbed as they associate with the formate ligands O−C−O backbone through weak electrostatic and other dispersion forces. This model is further supported by a DFT derived heatmap for H_2 positional energy inside the cavities of ALF. The heatmap suggests the existence of a shallow energy landscape for H_2 towards the walls of the LC, contrasting with a clear localized low energy landscape for H_2 positioned at the centre of the SC (Supporting Information). There is also excellent agreement between the total hydrogen capacity of the pores compared to that expected from the 160 K adsorption isotherm.

Furthermore, in agreement with our diffraction and isotherm results, the DFT calculated H_2 heats of adsorption for each of the cavities are found to be 11.66 kJ/mol and 12.54 kJ/mol for the SC and LC, respectively (details in Supporting Information). These similarly valued heat of adsorptions for the two cavities aligns well with what was seen from diffraction, which suggests that H_2 fills both cavities with comparable amounts, with a slight preference for the LC. The DFT calculated heat of adsorption values are also close to the isotherm-derived heat of adsorption of 8.67 kJ/mol (fitting from non-linear Langmuir fits to the adsorption data 120 K – 297 K, Figure S6). It is understood from the literature that the optimal heat of adsorption for hydrogen storage materials at ambient conditions should be between 15 kJ/mol and 25 kJ/mol.[9]

https://doi.org/10.26434/chemrxiv-2023-7b1m5 **ORCID:** https://orcid.org/0000-0002-1331-4274 Content not peer-reviewed by ChemRxiv. **License:** CC BY-NC-ND 4.0

Techno-economic analysis (TEA) of stationary long-duration H_2 storage using ALF

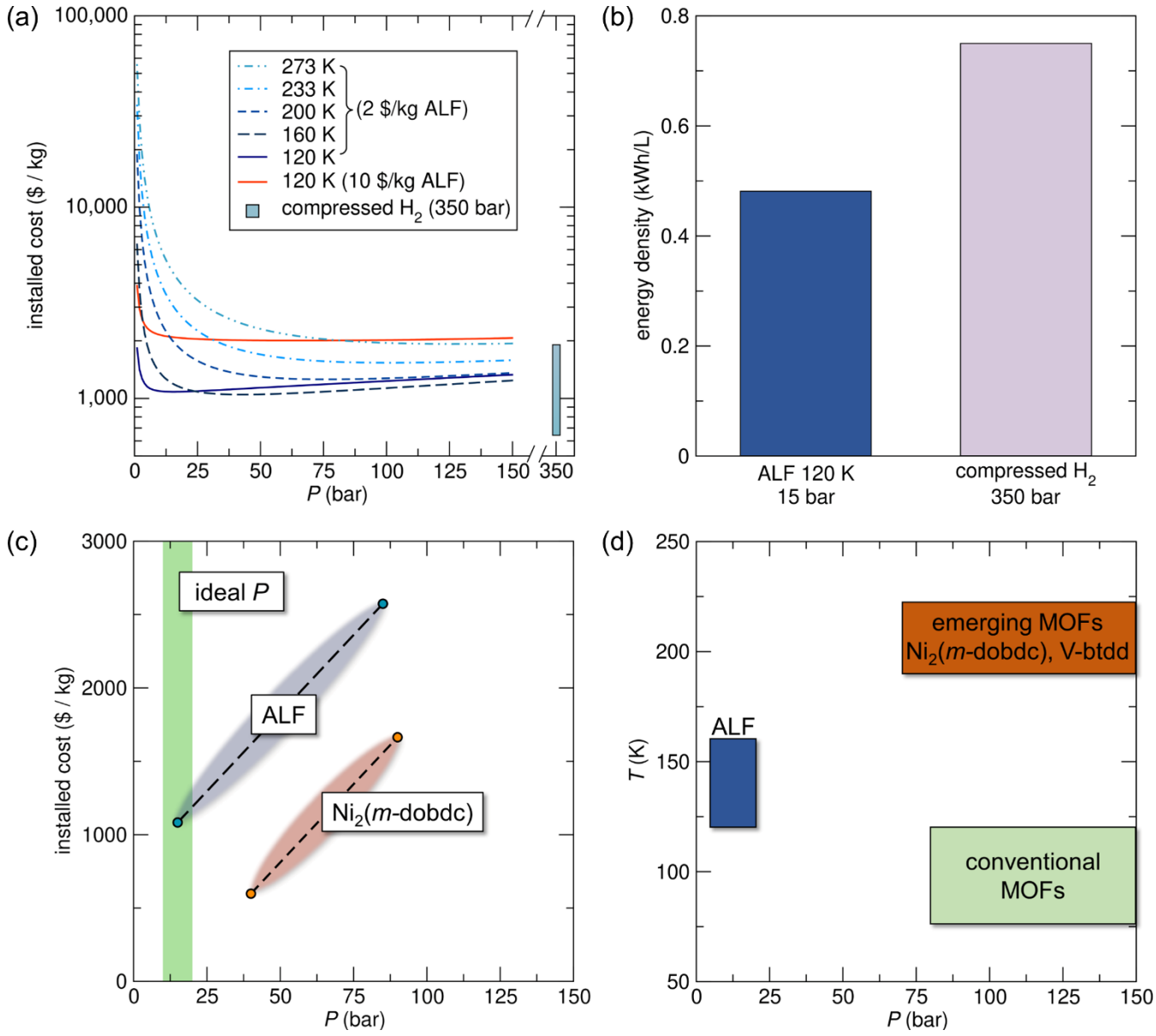

Figure 3. Technoeconomic analysis (TEA) and system-level performance of ALF versus compressed gas and other MOFs. a) Modeled installed capital cost for ALF at different temperatures and pressures, when charging rate is the same as discharge rate. The red line shows the installed cost if ALF was priced at 10 $/kg. Compressed gas installed costs at 350 bar are shown by the light blue bar. b) Comparison of system-level energy density of ALF with compressed hydrogen storage under 350 bar (293 K), calculated based on the amount of hydrogen stored in a tank and the tank's outer volume. c) Comparison of ALF with a top-performing contemporary MOF (Ni_2(*m*-dobdc)) under optimum cost and pressures under different manufacturing costs and operating conditions (low-cost value – 2 $/kg with moderate charging (charge = discharge) and high-cost value – 10 $/kg with fast charging (charge = 4 times faster than the discharge) for both MOFs). The green area denotes ideal delivery pressure range (10 bar – 20 bar) for stationary applications when coupled with fuel cells. Dashed lines between the two data points for ALF and Ni_2(*m*-dobdc) are used for easier comparison between the ranges. The shaded region behind the line denotes that values between the two ranges can vary. D) a schematic diagram depicting the optimum range of temperature and pressure conditions for different types of MOFs.

ALF distinguishes itself from most MOF materials proposed for long-duration H_2 storage by being derived from low-cost commodity chemicals and still achieving high H_2 uptakes at low working pressures and non-cryogenic temperatures. We evaluate the impact of these characteristics on the cost for an on-site, large-scale (10 MW) and long-duration (96 hours) stationary H_2 storage application. Low pressure operation is compelling, as a storage

https://doi.org/10.26434/chemrxiv-2023-7b1m5 **ORCID:** https://orcid.org/0000-0002-1331-4274 Content not peer-reviewed by ChemRxiv. **License:** CC BY-NC-ND 4.0

pressure between 10 bar to 25 bar is all that is needed for serving the pressure requirements of stationary fuel cells operating at 2 bar - 10 bar.[22] Beyond economic considerations, operating storage systems at low pressures also greatly reduces the safety concerns and system complexity when dispensing H_2, providing lower system costs and fostering general public acceptance of the technology.

With regard to material costs, at high manufacturing rates, it has been suggested that emerging MOFs that are manufactured using abundant metals, such as nickel or zinc, can achieve a material cost of 10 $/kg of MOF.[23] Lowering the MOF manufacture cost to the level of ≈2 $/kg, which is expected with ALF given that it is made from the abundant commodity chemical reagents aluminum hydroxide and formic acid (priced at 0.3-0.5 $/kg and 0.5-0.9 $/kg wholesale costs, respectively Supporting Information), provides a cost reduction with substantial promise. ALF avoids the use of comparatively complex organic reagents such as 2,5-dihydroxyterephthalic acid or metal salts such as nickel nitrate (priced at 2-20 $/kg and 3-15 $/kg, respectively, Supporting Information). Assuming a conservative material cost of 2 $/kg and based on the H_2 excess uptake with ALF (Figure 1) and its other fundamental properties (density, specific heat, etc.), we find that a minimum levelized cost of storage is achieved at a working pressure near 15 bar (Figure 3a). At this pressure and under moderate cooling (120 K), ALF achieves approximately two-thirds of the system-level energy density of 350 bar compressed gas storage at ambient conditions (Figure 3b). This represents a ≈95% pressure reduction for comparable performance when using ALF.

If such low material costs can be achieved, ALF offers a levelized cost of storage that is lower than 350 bar compressed gas systems, despite its cooling requirement (Figure 3a). This is true, even at a working temperature of 273 K; however, more pressure is required for ALF to achieve costs that are comparable with 350 bar compressed gas systems. A low material cost, such as ALF, would also put the capital cost of MOF on par with other system components, such as compressors and refrigerators (Supporting Information, Figure S15). We compare ALF to an emerging leader for H_2 storage, Ni_2(*m*-dobdc), to illustrate each material's optimal operation range based on their cost performance across 120 K - 293 K and 0 bar to 170 bar (Figure 3c). The findings are remarkable as both ALF and Ni_2(*m*-dobdc) could achieve a lower levelized cost of storage than 350 bar compressed gas systems. To our knowledge, this is the first study where sorbent-based hydrogen storage outperforms cryogenic and compressed gas technologies in a hydrogen storage application.

Lastly, the unique adsorption attributes of ALF compared to contemporary MOFs provide new opportunities for future applications for H_2 storage (Figure 3d). ALF's optimum conditions use moderate cooling and low pressures to achieve high storage, potentially making ALF suitable for applications where a precooled hydrogen stream requires storage, as may be the case for the capture of cryogenic boil-off gas capture.[24]

Conclusion

Herein, we have shown that aluminum formate, ALF, which adopts the ReO_3-type structure, adsorbs H_2 at non-cryogenic temperatures with an experimental heat of adsorption of ≈8.6 kJ/mol. From in-situ neutron diffraction analysis of D_2-dosed ALF, we show how both of ALF's cavities fill at comparable levels. Specifically, the large cavity of ALF has more localized D_2 molecules near the walls of the framework, whilst in the small cavity, D_2 molecules are located near the centre. The adsorption isotherms show that the optimal performance of ALF is found at relatively low pressures (around 25 bar) where the total uptake is near 12g H_2 / kg of ALF at 120 K. Most importantly, ALF's H_2 adsorption performance makes it unique compared to other reported MOFs for low pressure applications at intermediate temperatures.

From technoeconomic analysis, we have shown that ALF is currently the only MOF (to date) to achieve cost parity with 350 bar compressed gas storage at a working pressure within the ideal operation range for safe storage systems serving fuel cells. This is achieved at non-cryogenic temperatures, with the best cost performance found between 120 K and 160 K. Given its lower pressure adsorption performance, ALF also shows promise in emerging H_2 storage/capture areas of interest, such as H_2 boil-off capture. These results are impressive alone but are further

https://doi.org/10.26434/chemrxiv-2023-7b1m5 **ORCID:** https://orcid.org/0000-0002-1331-4274 Content not peer-reviewed by ChemRxiv. **License:** CC BY-NC-ND 4.0

amplified by the practical attributes of ALF for industrially relevant processes. First, ALF is pellitizable, as demonstrated previously,[11] contrasting many large void space MOFs that often amorphize upon pellitization.[25] Second, ALF is chemically robust, withstanding weeks at ambient air conditions without major degradation.[11] Lastly, as ALF is made from cheap and ubiquitous commodity chemicals, it faces fewer challenges in scalability compared to most other MOFs (note our previous demonstration of kilogram scale synthesis of ALF using laboratory methods[11]). Such characteristics are key for unlocking opportunities for sorbent-based hydrogen storage, as are the proper identification of market applications with sorbent behaviour and ideal operating conditions. As cooling adds refrigeration costs, ALF will benefit from applications where low-pressure and cool or near ambient hydrogen is available and requires storage.

Author Contributions

Writing – original draft: HAE. Writing – review & editing: HAE, TY, CBM, PP, HB, AKC. Formal analysis: HAE, TY, PP, HB, ZD, PC, CMB. Visualization: HAE. Conceptualization: HAE, TY, CBM. Investigation: HAE, TY, CBM, PP, HB, DM, ZD, YQ, QZ, PC, DM, DZ, AKC.

Conflicts of interest

A patent has been filed protecting certain information disclosed within this manuscript.

Acknowledgements

This work was partially supported by the following sources. We acknowledge NIST for partial funding for this work. The authors gratefully acknowledge partial support from the Hydrogen Materials—Advanced Research Consortium (HyMARC) established as part of the Energy Materials Network under the US DOE Office of Energy Efficiency and Renewable Energy (EERE), Hydrogen and Fuel Cell Technologies Office, under contract number DE-AC02-05CH11231 with Lawrence Berkeley National Laboratory (H.B., P.P). A portion of this research used resources at the Spallation Neutron Source [POWGEN], a DOE Office of Science User Facility operated by the Oak Ridge National Laboratory. Y.C. and Q.Z. thank Mark Loguillo and Matt Rucker for their assistance with sample environment setup. We a thank the Singapore MOE-Academic Research Fund (R-284-000-193-114) (DM, AKC), the National University of Singapore Green Energy Programme for partial funding under the project code R-284-000-185-731(AKC, DZ, PC), the Agency for Science, Technology and Research (U2102d2004) (DZ), and the Ras al Khaimah Centre for Advanced Materials (AKC). ZD thanks the support from his Lee Kuan Yew Postdoctoral Fellowship (22-5930- A0001). We thank Ryan Klein (NREL) for fruitful discussion. Certain commercial equipment, instruments, or materials are identified in this document. Such identification does not imply recommendation or endorsement by the National Institute of Standards and Technology, nor does it imply that the products identified are necessarily the best available for the purpose.

Associated Content.

The Supporting Information, which contains experimental details and supporting figures, is available free of charge at XXX.

Notes and references

(1) Goldsmith, J.; Wong-Foy, A. G.; Cafarella, M. J.; Siegel, D. J. Theoretical Limits of Hydrogen Storage in Metal–Organic Frameworks: Opportunities and Trade-Offs. *Chem. Mater.* **2013**, *25* (16), 3373–3382. https://doi.org/10.1021/cm401978e.

https://doi.org/10.26434/chemrxiv-2023-7b1m5 **ORCID:** https://orcid.org/0000-0002-1331-4274 Content not peer-reviewed by ChemRxiv. **License:** CC BY-NC-ND 4.0

(2) Hunter, C. A.; Penev, M. M.; Reznicek, E. P.; Eichman, J.; Rustagi, N.; Baldwin, S. F. Techno-Economic Analysis of Long-Duration Energy Storage and Flexible Power Generation Technologies to Support High-Variable Renewable Energy Grids. *Joule* **2021**, *5* (8), 2077–2101. https://doi.org/10.1016/j.joule.2021.06.018.
(3) Ma, Z.; Eichman, J.; Kurtz, J. Fuel Cell Backup Power System for Grid Service and Microgrid in Telecommunication Applications. *J. Energy Resour. Technol.* **2019**, *141* (6), 062002. https://doi.org/10.1115/1.4042402.
(4) Peng, P.; Anastasopoulou, A.; Brooks, K.; Furukawa, H.; Bowden, M. E.; Long, J. R.; Autrey, T.; Breunig, H. Cost and Potential of Metal–Organic Frameworks for Hydrogen Back-up Power Supply. *Nat. Energy* **2022**, *7* (5), 448–458. https://doi.org/10.1038/s41560-022-01013-w.
(5) Haug, P.; Kreitz, B.; Koj, M.; Turek, T. Process Modelling of an Alkaline Water Electrolyzer. *Int. J. Hydrog. Energy* **2017**, *42* (24), 15689–15707. https://doi.org/10.1016/j.ijhydene.2017.05.031.
(6) Gómez-Gualdrón, D. A.; Colón, Y. J.; Zhang, X.; Wang, T. C.; Chen, Y.-S.; Hupp, J. T.; Yildirim, T.; Farha, O. K.; Zhang, J.; Snurr, R. Q. Evaluating Topologically Diverse Metal–Organic Frameworks for Cryo-Adsorbed Hydrogen Storage. *Energy Environ. Sci.* **2016**, *9* (10), 3279–3289. https://doi.org/10.1039/C6EE02104B.
(7) Bobbitt, N. S.; Chen, J.; Snurr, R. Q. High-Throughput Screening of Metal–Organic Frameworks for Hydrogen Storage at Cryogenic Temperature. *J. Phys. Chem. C* **2016**, *120* (48), 27328–27341. https://doi.org/10.1021/acs.jpcc.6b08729.
(8) Kapelewski, M. T.; Runčevski, T.; Tarver, J. D.; Jiang, H. Z. H.; Hurst, K. E.; Parilla, P. A.; Ayala, A.; Gennett, T.; FitzGerald, S. A.; Brown, C. M.; Long, J. R. Record High Hydrogen Storage Capacity in the Metal–Organic Framework Ni_2(m-Dobdc) at near-Ambient Temperatures. *Chem. Mater.* **2018**, *30* (22), 8179–8189. https://doi.org/10.1021/acs.chemmater.8b03276.
(9) Jaramillo, D. E.; Jiang, H. Z. H.; Evans, H. A.; Chakraborty, R.; Furukawa, H.; Brown, C. M.; Head-Gordon, M.; Long, J. R. Ambient-Temperature Hydrogen Storage via Vanadium(II)-Dihydrogen Complexation in a Metal–Organic Framework. *J. Am. Chem. Soc.* **2021**, *143* (16), 6248–6256. https://doi.org/10.1021/jacs.1c01883.
(10) Evans, H. A.; Wu, Y.; Seshadri, R.; Cheetham, A. K. Perovskite-Related ReO_3-Type Structures. *Nat. Rev. Mater.* **2020**, *5* (3), 196–213. https://doi.org/10.1038/s41578-019-0160-x.
(11) Evans, H. A.; Mullangi, D.; Deng, Z.; Wang, Y.; Peh, S. B.; Wei, F.; Wang, J.; Brown, C. M.; Zhao, D.; Canepa, P.; Cheetham, A. K. Aluminum Formate, $Al(HCOO)_3$: An Earth-Abundant, Scalable, and Highly Selective Material for CO_2 Capture. *Sci. Adv.* **2022**, *8* (44), eade1473. https://doi.org/10.1126/sciadv.ade1473.
(12) Zhang, Z. Exclusive Recognition of CO_2 from Hydrocarbons by Aluminum Formate with Hydrogen-Confined Pore Cavities. *J. Am. Chem. Soc.* **2023**. https://doi.org/10.1021/jacs.3c01705.
(13) Mullangi, D.; Evans, H. A.; Yildirim, T.; Wang, Y.; Deng, Z.; Zhang, Z.; Mai, T. T.; Wei, F.; Wang, J.; Hight Walker, A. R.; Brown, C. M.; Zhao, D.; Canepa, P.; Cheetham, A. K. Noncryogenic Air Separation Using Aluminum Formate $Al(HCOO)_3$ (ALF). *J. Am. Chem. Soc.* **2023**, *145* (17), 9850–9856. https://doi.org/10.1021/jacs.3c02100.
(14) Linstrom, P. J.; Mallard, W. G. *NIST Chemistry WebBook, NIST Standard Reference Database Number 69*; National Institute of Standards and Technology.
(15) Breck, D. W.; Eversole, W. G.; Milton, R. M.; Reed, T. B.; Thomas, T. L. Crystalline Zeolites. I. The Properties of a New Synthetic Zeolite, Type A. *J. Am. Chem. Soc.* **1956**, *78* (23), 5963–5972. https://doi.org/10.1021/ja01604a001.
(16) Kim, H.; Samsonenko, D. G.; Yoon, M.; Yoon, J. W.; Hwang, Y. K.; Chang, J.-S.; Kim, K. Temperature-Triggered Gate Opening for Gas Adsorption in Microporous Manganese Formate. *Chem. Commun.* **2008**, No. 39, 4697–4699. https://doi.org/10.1039/B811087E.
(17) Brown, C. M.; Liu, Y.; Yildirim, T.; Peterson, V. K.; Kepert, C. J. Hydrogen Adsorption in HKUST-1: A Combined Inelastic Neutron Scattering and First-Principles Study. *J. Energy Resour. Technol.* **2009**, *20*, 204025. https://doi.org/10.1088/0957-4484/20/20/204025.
(18) Pollock, R. A.; Her, J.-H.; Brown, C. M.; Liu, Y.; Dailly, A. Kinetic Trapping of D_2 in MIL-53(Al) Observed Using Neutron Scattering. *J. Phys. Chem. C* **2014**, *118* (31), 18197–18206. https://doi.org/10.1021/jp504870n.
(19) Wu, H.; Zhou, W.; Yildirim, T. Hydrogen Storage in a Prototypical Zeolitic Imidazolate Framework-8. *J. Am. Chem. Soc.* **2007**, *129* (17), 5314–5315. https://doi.org/10.1021/ja0691932.

https://doi.org/10.26434/chemrxiv-2023-7b1m5 **ORCID:** https://orcid.org/0000-0002-1331-4274 Content not peer-reviewed by ChemRxiv. **License:** CC BY-NC-ND 4.0

(20) Barnett, B. R.; Evans, H. A.; Su, G. M.; Jiang, H. Z. H.; Chakraborty, R.; Banyeretse, D.; Hartman, T. J.; Martinez, M. B.; Trump, B. A.; Tarver, J. D.; Dods, M. N.; Funke, L. M.; Börgel, J.; Reimer, J. A.; Drisdell, W. S.; Hurst, K. E.; Gennett, T.; FitzGerald, S. A.; Brown, C. M.; Head-Gordon, M.; Long, J. R. Observation of an Intermediate to H_2 Binding in a Metal–Organic Framework. *J. Am. Chem. Soc.* **2021**, *143* (36), 14884–14894. https://doi.org/10.1021/jacs.1c07223.

(21) Klein, R. A.; Evans, H. A.; Trump, B. A.; Udovic, T. J.; Brown, C. M. 10.02 - Neutron Scattering Studies of Materials for Hydrogen Storage. In *Comprehensive Inorganic Chemistry III (Third Edition)*; Reedijk, J., Poeppelmeier, K. R., Eds.; Elsevier: Oxford, 2023; pp 3–50. https://doi.org/10.1016/B978-0-12-823144-9.00028-5.

(22) Wong, C. Y.; Wong, W. Y.; Ramya, K.; Khalid, M.; Loh, K. S.; Daud, W. R. W.; Lim, K. L.; Walvekar, R.; Kadhum, A. A. H. Additives in Proton Exchange Membranes for Low- and High-Temperature Fuel Cell Applications: A Review. *Int. J. Hydrog. Energy* **2019**, *44* (12), 6116–6135. https://doi.org/10.1016/j.ijhydene.2019.01.084.

(23) DeSantis, D.; Mason, J. A.; James, B. D.; Houchins, C.; Long, J. R.; Veenstra, M. Techno-Economic Analysis of Metal–Organic Frameworks for Hydrogen and Natural Gas Storage. *Energy Fuels* **2017**, *31* (2), 2024–2032. https://doi.org/10.1021/acs.energyfuels.6b02510.

(24) Petitpas, G. *Boil-off Losses along LH2 Pathway*; LLNL-TR-750685; Lawrence Livermore National Lab. (LLNL), Livermore, CA (United States), 2018. https://doi.org/10.2172/1466121.

(25) Tan, J. C.; Cheetham, A. K. Mechanical Properties of Hybrid Inorganic–Organic Framework Materials: Establishing Fundamental Structure–Property Relationships. *Chem. Soc. Rev.* **2011**, *40* (2), 1059–1080. https://doi.org/10.1039/C0CS00163E.

https://doi.org/10.26434/chemrxiv-2023-7b1m5 **ORCID:** https://orcid.org/0000-0002-1331-4274 Content not peer-reviewed by ChemRxiv. **License:** CC BY-NC-ND 4.0